nature communications

Article

https://doi.org/10.1038/s41467-025-57779-6

Recapitulating hypoxic metabolism in cartilaginous organoids via adaptive cell-matrix interactions enhances histone lactylation and cartilage regeneration

Received: 29 July 2024

Accepted: 4 March 2025

Published online: 19 March 2025

Check for updates

Boguang Yang[1,2,8], Zhuo Li[1,8], Zhengmeng Yang[2,8], Pengchao Zhao[3,4,5], Sien Lin[2], Jiahao Wu[6], Wei Liu[6], Xuefeng Yang[1,7], Xian Xie[1], Zhixian Zong[2], Yuanning Lyu[3,4,5], Zhinan Yang[1], Gang Li[2], To Ngai[6] ✉, Kunyu Zhang[3,4,5] ✉ & Liming Bian[3,4,5] ✉

Mesenchymal condensation, characterized by rapid proliferation and aggregation of precursor cells within a restructured mesodermal extracellular matrix, is critical for skeletal tissue development, including articular cartilage. This process establishes a hypoxic microenvironment that drives metabolic shifts and epigenetic modifications essential for cartilage development. To replicate this, we engineer a cell-adaptable supramolecular hydrogel that accommodates the extensive volumetric and morphological changes of encapsulated mesenchymal stromal cells, facilitating the rapid formation of large multicellular cartilaginous organoids. This adaptation fosters a hypoxic environment and induces metabolic shifts toward glycolysis, increasing lactate accumulation and histone lysine lactylation. Enhanced lactylation on Lysine 18 of Histone H3 promotes chondrogenesis and cartilage matrix deposition by improving the accessibility of chondrogenic genes, while the inhibition of histone lactylation disrupts these processes. Implantation of the ultradynamic hydrogel in large animal cartilage defects results in superior repair compared to less dynamic alternatives, providing insights for effective biomaterial delivery in cell therapies. Our findings reveal how matrix biophysical cues influence cellular development, metabolic reprogramming, and epigenetic modifications.

The biophysical cues in the three-dimensional (3D) cell microenvironment, such as the mechanical properties of the extracellular matrix (ECM), play a vital role in regulating cell behaviors, including proliferation, metabolism, and differentiation[1–3]. Hydrogels have been widely studied to emulate the biophysical properties of the ECM to serve as the delivery vehicle of therapeutic cells for repairing injured soft tissue such as articular cartilage[4–6]. However, conventional covalently crosslinked hydrogels generally possess limited network dynamics and cannot accommodate the extensive volumetric changes involved in the rapid proliferation and extensive aggregation of the encapsulated cells. This limits the formation of cartilaginous organoids and the outcomes of cartilage repair. In contrast, previous studies have demonstrated that the dynamic mechanical properties of hydrogels can have significant impact on the behaviors of encapsulated cells[7,8]. A recent study demonstrated that hydrogels with fast stress relaxation can provide a more conducive microenvironment to enhance

A full list of affiliations appears at the end of the paper. ✉e-mail: tongai@cuhk.edu.hk; kyuzhang@scut.edu.cn; bianlm@scut.edu.cn

cartilaginous matrix deposition by chondrocytes, whereas hydrogels with slower relaxation restricted cell and matrix volume expansion under elastic stress[4]. Another study showed that more viscoelastic hydrogels facilitated cartilaginous ECM deposition by encapsulated chondrocytes[5]. Meanwhile, mesenchymal stromal/stem cells (MSCs), a promising cell source for cartilage repair, require complex development-conducive matrix biophysical cues for chondrogenesis. Therefore, examining the impact of dynamic biophysical properties of ECM on cartilage precursor cells during the cartilage template development can provide critical inspiration for the design of biomimetic hydrogels to enhance MSC chondrogenesis.

Mesenchymal condensation is a critical early event of cartilage template development, during which the dispersed precursor cells rapidly reorganize the surrounding mesoderm ECM to proliferate and aggregate at high cell density, thereby establishing the hypoxic microenvironment required for chondrogenesis[9–12]. Therefore, developing hydrogels with the ultradynamic cell adaptable structure to facilitate the mesenchymal condensation and hypoxic metabolism of encapsulated MSCs holds great significance for the construction of cartilaginous organoids and cartilage regeneration. However, MSCs seeded in conventional hydrogels with low network dynamics generally do not form cell condensates of significant size because insufficient network dynamics cannot accommodate the rapid and drastic volumetric expansion accompanying the excessive cell proliferation and migration required for cell aggregation. Therefore, the development of hydrogel carriers, which can support the rapid proliferation and extensive aggregation of encapsulated MSCs, is essential for providing a biomimetic 3D microenvironment for mesenchymal condensation to enhance formation of cartilaginous organoids and cartilage repair[5,13]. This requires that the hydrogels possess an ultradynamic cell-adaptable network to dissipate the stress generated by the rapidly expanding cellular mass and ECM of encapsulated cells via dynamic disruption/reorganization of the hydrogel network in a timely manner.

Herein, we fabricate an ultradynamic hydrogel physically crosslinked by host–guest complexation between *p*-tert-butylphenyl-modified hyaluronic acid (HA-TP) and β-cyclodextrin. The Brownian movement of the encapsulated nanoparticles is an indication of the level of network dynamics in the hydrogel. Micro-rheological analysis shows that the nanoparticles entrapped in the HA-TP hydrogel travel significantly further distances through Brownian motion within the same timeframe compared with the cholic acid-modified hyaluronic acid (HA-CA) hydrogel, indicating the higher level of network dynamics in HA-TP hydrogel[14,15]. The cell-adaptable dynamic network of the HA-TP hydrogel substantially promotes the proliferation, migration and organoids formation of encapsulated human MSCs (hMSCs), whereas the limited network dynamics of the control hydrogel restrict cell spheroid development. By emulating mesenchymal condensation during cartilage development, the HA-TP hydrogel supports significant cell organoids formation, which creates a hypoxic local microenvironment and drives the metabolic switch, resulting in increased lactate accumulation and enhanced histone lactylation in the encapsulated hMSCs. We further show that enhanced histone lactylation promotes the chondrogenic differentiation of the hMSCs encapsulated in the ultradynamic hydrogel, and to the best of our knowledge, this has not been reported before (Fig. 1). Both the delivery of MSCs by the ultradynamic HA-TP hydrogel and application of lyophilized HA-TP hydrogel sponge effectively promote the rapid regeneration of hyaline cartilage and subchondral bone in the animal articular cartilage defect models. Our findings highlight the critical importance of designing a cell-adaptable dynamic hydrogel network to facilitate the developmentally required condensation and metabolic reprogramming of encapsulated cells, thereby enhancing the formation of cartilaginous organs and promoting in situ tissue regeneration.

Results and discussion

Ultra-dynamic hydrogel containing physical crosslink with high binding/dissociation kinetics promotes cartilaginous organoids formation

To study the effects of hydrogel structural dynamics on chondrogenesis of encapsulated hMSCs, we employed two host–guest complexations, β-cyclodextrin–4-tert-butylphenyl (CD–TP) and β-cyclodextrin–cholic acid (CD–CA), as physical crosslinks to fabricate

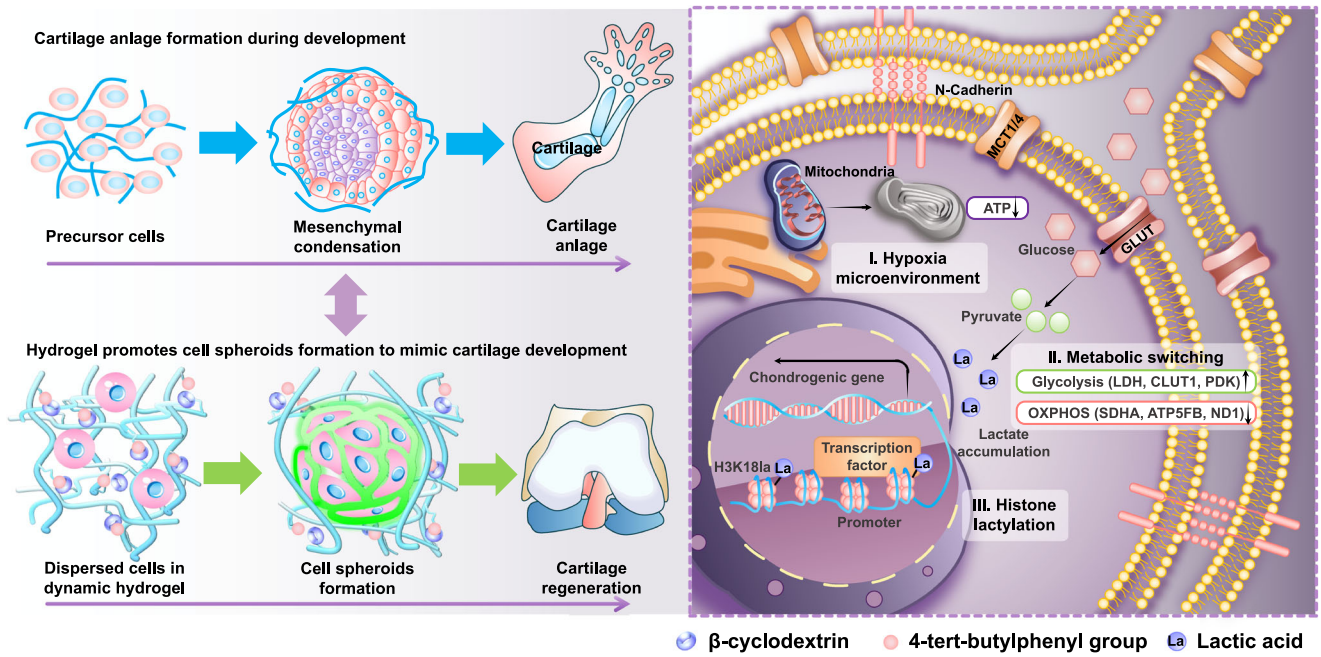

Fig. 1 | Cell-adaptable dynamic hydrogel network facilitates the developmentally required condensation and metabolic reprogramming of encapsulated cells to enhance the formation of cartilaginous organs and promote in situ tissue regeneration. The dynamic HA-TP hydrogel induces hMSC condensation formation to mimic the natural chondrogenesis process and promotes the secretion of lactic acid, which drives specific histone lactylation at promoters of chondrogenesis-related genes, thereby promoting the formation of cartilaginous organoids.

supramolecular HA-TP and HA-CA hydrogels, respectively (Fig. 2a and Supplementary Fig. 1). Scanning electron microscopy images revealed the similar uniform porous structure in both hydrogels (Supplementary Fig. 2). Microrheology analysis based on tracking the polystyrene nanoparticles (600 nm diameter) encapsulated in the hydrogels was used to investigate the microscopic network dynamics of the two hydrogels. At room temperature, the mean-squared displacement (MSD) of polystyrene nanoparticles in the HA-TP hydrogel increased almost linearly with time (Fig. 2b, pink curve), whereas the MSD curve of the HA-CA hydrogel quickly plateaued with time (Fig. 2b, blue curve). This finding showed that the HA-TP hydrogel can support significantly more Brownian movement of entrapped nanoparticles than the HA-CA hydrogel, thereby indicating the higher microscopic network dynamics of the HA-TP hydrogel[16]. Consistent with the microrheological data, the frequency sweep analysis (10^{-3} Hz to 10^{1} Hz) showed that the storage modulus value (G') of the HA-TP hydrogel exhibited a stronger frequency dependence than that of the HA-CA hydrogel (Supplementary Fig. 3a). In addition, the HA-TP hydrogel showed a markedly shorter half-stress relaxation time ($\tau_{1/2}$ ~ 9.7 s) than the HA-CA hydrogel ($\tau_{1/2}$ ~ 38.9 s) in response to 15% compression (Supplementary Fig. 3b, c). At a set frequency (0.1 Hz), the two types of physically crosslinked hydrogels possessed similar storage modulus values (G' ~ 1000 Pa), while the loss modulus of HA-TP hydrogels (G'' ~ 298 Pa) was significantly higher than that of HA-CA hydrogels (G'' ~ 36 Pa) (Supplementary Fig. 3c). We further examined the movement of magnetic beads ($Ø$ = 4.5 μm, simulating cell size) in hydrogels under an oscillating magnetic force of 25.5 pN (at a frequency of 0.2 Hz via magnetic tweezer) by measuring the scattering intensity of the incident laser[17]. Scattering intensity data revealed that the magnetic beads in the HA-TP hydrogel exhibited regular periodic motion under the influence of the magnetic force (Fig. 2c and Movie S1), whereas the beads in the HA-CA hydrogel remained immobilized due to the relatively static crosslinking of the network (Fig. 2c and Movie S2). These findings together demonstrate the ultra-dynamic network of the HA-TP hydrogel, which is not found in the HA-CA hydrogel[8].

Surface plasmon resonance (SPR) was employed to investigate the kinetic binding constants and thermodynamic equilibrium constants of the two host–guest complexations (Fig. 2d). The sensorgrams showed the rapid binding of soluble HA-TP to the cyclodextrin immobilized on the chip surface untill reaching equilibrium within 10 s upon the start of HA-TP solution flow, while the amount of bound HA-TP rapidly decreased after the cessation of the flow. In contrast, the amount of bound HA-CA increased gradually after the flow started, failing to reach equilibrium even after 200 s, and subsequently decreased slowly upon the cessation of flow (Fig. 2d). Based on the curvefitting and calculations, the kinetic binding constant of the more dynamic host–guest complexation (HA-TP and CD) were determined to be significantly higher ($k_{on,TP} = 1.23 \times 10^5$ 1/Ms, $k_{off,TP} = 1.77 \times 10^{-2}$ 1/s) than those of the less dynamic complexation (HA-CA and CD) ($k_{on,CA} = 1.73 \times 10^3$ 1/Ms, $k_{off,CA} = 1.47 \times 10^{-3}$ 1/s), while there is no significant difference in the dissociation thermodynamic constants ($K_D = k_{off}/k_{on}$) of these two pairs of host–guest complexations (Fig. 2e and Supplementary Fig. 3d). This result indicates that the HA-TP hydrogel possesses a more dynamic crosslinking structure compared to the HA-CA hydrogel, and this is consistent with the differential dynamic mechanical properties of the two hydrogels. Human mesenchymal stromal/stem cells (hMSCs) were encapsulated as dispersed single cells in the HA-TP and HA-CA hydrogels and cultured under chondrogenic conditions for 5 days. SEM analysis of cross-sections of the cell-loaded hydrogels revealed the formation of large multi-cellular cartilaginous organoids in the HA-TP hydrogel (Fig. 2f). In contrast, cells within the HA-CA hydrogel remained as the isolated individual round cells without significant aggregation and proliferation (Fig. 2f). After 10 days of chondrogenic culture, the cartilaginous organoids retrieved by degrading the HA-TP hydrogel showed good cellular viability (Supplementary Fig. 4). These findings suggest that compared with that of the HA-CA hydrogel, the ultra-dynamic network structure of HA-TP hydrogel can better accommodate the excessive volumetric expansion associated with the aggregation and proliferation of encapsulated cells during the cartilaginous organoids formation.

Ultra-dynamic hydrogel promotes cell–cell interactions and the formation of cartilaginous organoids by encapsulated hMSCs

Previous studies suggested that multicellular MSC spheroids exhibit enhanced chondrogenesis and limited fibrosis, thereby favouring hyaline cartilage regeneration[18,19]. We encapsulated hMSCs in the HA-TP and HA-CA hydrogels to study the effect of hydrogel network dynamics on the development of cartilaginous organoids by the encapsulated hMSCs. After culture for only 3 days in chondrogenic medium, the initially isolated cells proliferated extensively to form visible cartilaginous organoids in the HA-TP hydrogel (Fig. 3a, b). On day 5, each organoid in the HA-TP hydrogel contained ~10–20 cells. In contrast, most hMSCs encapsulated in the HA-CA hydrogel remained isolated single cells (Fig. 3a, b). The average size of the cell organoids (maximal cross-sectional area based on confocal images) in the more dynamic HA-TP hydrogel (~3500 μm^2) was ~10-fold larger than that in the less dynamic HA-CA hydrogel (~300 μm^2) (Supplementary Fig. 5). To further investigate the mechanisms of spheroid formation, cell proliferation was examined by nuclear division marker (EdU) staining. The percentage of EdU$^+$ cells in the HA-TP hydrogel was ~89% on Day 3 and gradually decreased over time, likely due to differentiation, while only ~20% EdU$^+$ cells were detected in the HA-CA hydrogel at all time points (Fig. 3a, b). Apart from the impact of the dynamics of the crosslinking structure on cell clusters, the initial cell seeding density is also an important factor influencing the size of the cell clusters. We cultured hMSCs in the HA-TP hydrogels at varying densities (1×10^7 cells/mL and 5×10^7 cells/mL), and the results showed a significant increase in cluster size as the initial seeding density increased, illustrating that higher seeding densities support larger cell clusters in the dynamic HA-TP matrix. It is well known that cell seeding density has a significant impact on cell clustering and spreading. In this study, we employed a moderate density of 1×10^7 cells/mL, which promoted robust cell proliferation and clustering without extensive inter-cluster interaction. Increasing the density to 5×10^7 cells/mL resulted in the formation of more interconnected cell clusters (Supplementary Fig. 6). We believe this is due to the increased ECM deposition with high cell seeding density, which facilitates cell migration and aggregation. These data suggest that at lower cell densities the dynamic hydrogel promoted the proliferation-driven cell spheroid formation, while increasing the seeding densities can expedite ECM deposition and cell migration, thereby promoting the formation of more interconnected cell spheroids. These data suggest that the more dynamic HA-TP hydrogel can better support the proliferation of encapsulated hMSCs to form multicellular cartilaginous organoids than the less dynamic HA-CA hydrogel.

Previous studies have identified a critical event in the chondrogenesis of stem cells and cartilage development[20–23]. Our immunofluorescence staining showed that N-cadherin expression in cartilaginous organoids formed in the more dynamic HA-TP hydrogel was significantly upregulated compared with that in the less dynamic HA-CA hydrogel at early time points (Days 3 and 5) (Fig. 3c). On Day 9, the N-cadherin expression in the HA-TP hydrogel diminished as the hMSCs differentiated to deposit an increasing amount of cartilaginous ECM, and this is consistent with previous reports of decreasing N-cadherin expression during chondrogenesis progression[24]. Interestingly, the hMSCs in the less dynamic HA-CA hydrogel showed only slight N-cadherin expression after 9 days of chondrogenic induction due to late and impaired development of cartilaginous organoids (Fig. 3c). These findings indicate that the higher network dynamics in

https://doi.org/10.1038/s41467-025-57779-6

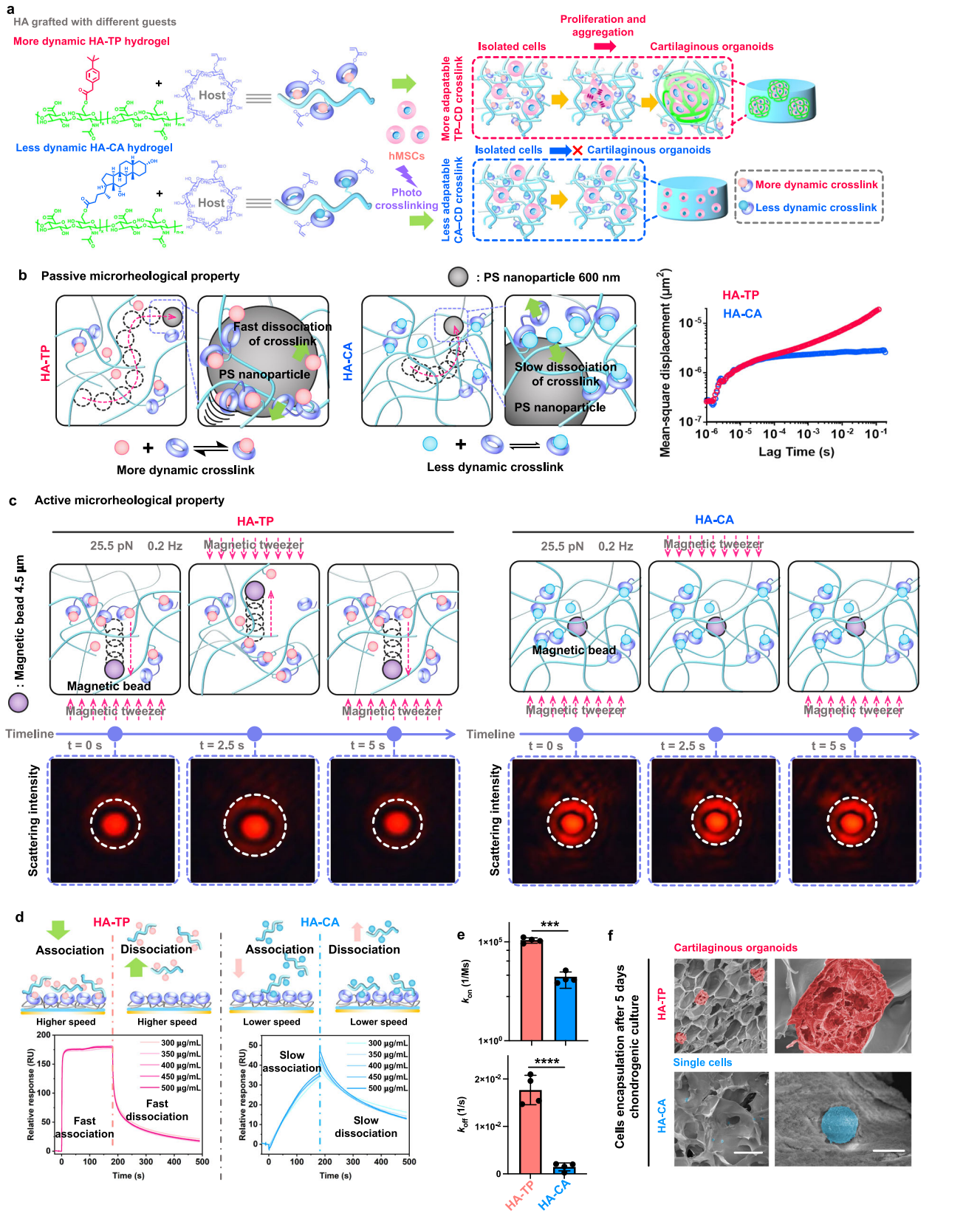

the HA-TP hydrogel expedited N-cadherin-mediated cell condensation and intercellular interactions, thereby promoting subsequent cartilaginous organoids development of the encapsulated hMSCs compared with the less dynamic HA-CA hydrogel. We encapsulated the cells in HA-TP hydrogels and cultured them for 14 days. The boundaries of the hydrogels remained intact, indicating minimal degradation (Supplementary Fig. 7). Besides, compared to previous results obtained after 10 days of culture, there was no significant change in the size of the cell clusters. This is likely because the hMSCs in chondrogenic culture medium continue to differentiate, and the differentiation reduces the proliferative capacity of the hMSCs, preventing further increase in the size of the cell clusters.

Fig. 2 | Supramolecular hydrogels stabilized by different host–guest crosslinks with different binding properties possess differential network dynamic properties. a Schematic illustration of the preparation of supramolecular hyaluronic acid hydrogels stabilized by different pairs of host–guest complexes (cyclodextrin–*p*-tert butylphenyl (CD–TP) vs. cyclodextrin–cholic acid (CD–CA)) and the differential cartilaginous organoids development of hMSCs encapsulated in the obtained HA-TP and HA-CA hydrogels. **b** The mean-square displacement (MSD) measured for the HA-TP and HA-CA hydrogels (4% w/v HA content) encapsulated with 1.5% (vol/vol) sterically stabilized PS tracer nanoparticles (600 nm diameter). **c** The magnetic bead probes dispersed in hydrogel were subject to an oscillating magnetic field (dashed lines). The scattering intensity of the bead probes generated by the incident laser was captured by a photomultiplier. The intensity of light scattering from the beads in the HA-TP hydrogel exhibits fluctuations, increasing and decreasing with their vertical movement. In contrast, the intensity of light scattering in the HA-CA hydrogel remains constant because the beads are constrained and unable to move significantly. **d** The SPR sensorgrams demonstrating the differential binding and unbinding kinetics of soluble HA-TP and HA-CA at varying concentrations (from top to bottom: 300, 350, 400, 450, 500 μg/ml) to CD immobilized on detection chips. **e** The k_{on} and k_{off} values between HA-TP and HA-CA with β-CD obtained through SPR experiments. Data are presented as mean values ± SD, $n = 4$ independent polymer samples per group; $^{***}p < 0.001$, $^{****}p < 0.0001$ (two-tailed Student's *t*-test). **f** Scanning electron microscopy results of the cross-sections of HA-TP and HA-CA hydrogel encapsulated with hMSCs after 5 days of chondrogenic induced culture. Scale bar: left column, 100 μm, right column, 15 μm.

To demonstrate that the dynamic hydrogel enhanced the deposition of cartilaginous matrix components in the cartilaginous organoids, we examined the expression of type II collagen and aggrecan, two well-known chondrogenic markers[25,26], in hMSCs encapsulated in the two hydrogels. After culture in chondrogenic medium for 10 days, the cartilaginous organoids in the HA-TP hydrogel deposited significantly more type II collagen and aggrecan than the single cells in the HA-CA hydrogel (Fig. 3d). In addition, Safranin O and Toluidine Blue staining revealed much more intense staining of cartilaginous proteoglycans in the HA-TP hydrogel than in the HA-CA hydrogel (Fig. 3d). Consistent with the staining results, qPCR data showed that the cartilaginous organoids in the HA-TP hydrogel had ~10-fold higher expression of *Sox9* and ~100-fold higher *Aggrecan* than the single hMSCs in the HA-CA hydrogel (Fig. 3e). Quantitative analysis of glycosaminoglycan (GAG) content revealed significantly higher GAG content of the HA-TP hydrogel group compared with that in the HA-CA hydrogel group (Supplementary Fig. 8). To evaluate the hypertrophic differentiation of the chondrogenically induced hMSCs in our dynamic hydrogels, hMSC-seeded hydrogels were further cultured in hypertrophy induction media for 5 days after 10 days of culture in chondrogenic medium. The expression of hypertrophy markers, including type X collagen and matrix metalloproteinase 13 (MMP 13), was hardly observed in the hydrogels with fast and slow dynamics (Fig. 3f and Supplementary Fig. 9). The lower expression of hypertrophy markers in the HA-CA hydrogel is likely due to the poor chondrogenic differentiation of single cells[27]. This finding suggested that the formation of cartilaginous organoids in the HA-TP hydrogel suppresses hypertrophic differentiation, and the exact mechanism remains to be further elucidated. These findings together indicate that the more dynamic HA-TP hydrogel can better promote the formation of cartilaginous organoids by the encapsulated hMSCs compared with the HA-CA hydrogel by supporting the proliferation and migration of the hMSCs.

Hypoxic microenvironment created in the cartilaginous organoids drives metabolic switching favorable for chondrogenesis

Cartilage is an avascular tissue, and thus chondrocytes reside in a microenvironment with reduced oxygen tension[28,29]. Previous studies have shown that hypoxia stimulates chondrogenic differentiation of MSCs and plays a critical role in driving articular cartilage formation[30–32]. By using Image-iT green, a probe that becomes fluorescent when oxygen levels are decreased, we showed a clear increase in the size of the hypoxic region in the center of growing cartilaginous organoids in the HA-TP hydrogels during the 7 days of chondrogenic culture (Fig. 4a). In contrast, the single cells in the HA-CA hydrogels, which failed to form significant spheroids, showed minimal signs of hypoxia (Fig. 4a). These findings indicate that the enhanced hMSCs condensation formation enabled by the higher network dynamics in the HA-TP hydrogel establishes a hypoxic microenvironment for the cells in the interior of the condensations, which promotes the formation of cartilaginous organoids[33].

Previous studies have shown that hypoxia is associated with defective mitochondrial functions and related metabolic programming during cellular differentiation processes[34–36]. As shown by transmission electron microscopy, the cells in the interior of the cartilaginous organoids in the HA-TP hydrogel exhibited a striking alteration in mitochondrial morphology, with fewer and shorter cristae per mitochondrion (Fig. 4b). In contrast, normal mitochondrial cristae were observed in the peripheral cells of the cartilaginous organoids in the HA-TP hydrogel and the single cells in the HA-CA hydrogel (Fig. 4b). Therefore, these results indicate that the hypoxic microenvironment established in the cartilaginous organoids interior in the HA-TP hydrogel can alter the morphology and function of mitochondria, and this is crucial to driving the metabolic switch of encapsulated hMSCs[33].

Previous studies have established that hypoxia mediates its effect largely through the transcriptional complex HIF-1 (hypoxia-inducible factor, containing the HIF-1α subunit), which binds to specific hypoxia-responsive elements, thereby initiating the transcription of target genes, such as *Sox9* or *Aggrecan*[37]. The immunofluorescence staining results showed a significant time-dependent increase in HIF-1α expression in the growing cartilaginous organoids in the HA-TP hydrogel (Fig. 4c), but HIF-1α expression was hardly observed in the single cells in the HA-CA hydrogel (Supplementary Fig. 10). Consistent with the results from immunofluorescence staining, the qPCR data showed significantly upregulated gene expression of *HIF-1α* in the cells in the HA-TP hydrogel compared with that in the HA-CA hydrogel (Supplementary Fig. 11). These findings further elucidate the mechanism by which the HA-TP hydrogel promotes the formation of cartilaginous organoids. The higher network dynamics of the HA-TP hydrogel facilitate the proliferation and migration of the encapsulated hMSCs, leading to the formation of cell condensations. Concurrently, a hypoxic microenvironment is established within these cell condensations, which upregulates the expression of HIF-1α. The increased expression of HIF-1α in turn enhances the induction of the chondrogenic transcription factor Sox9, which plays a critical role in the formation of the cartilaginous organoids. Thus, the HA-TP hydrogel with its highly dynamic network recapitulates the developmental process of cartilage formation by orchestrating the steps of cell condensation, hypoxic signaling, and chondrogenic differentiation[30].

According to previous studies, low oxygen tension drives the chondrogenic differentiation of MSCs through metabolic reprogramming[29]. After 3 days of culture in chondrogenic medium, the cartilaginous organoids in the HA-TP hydrogel showed higher expression of *glucose transporter 1* (*GLUT1*), *hexokinase* (*HK*) and *pyruwate dehydrogenase kinase* (*PDK*), key markers of glycolysis, than the single hMSCs in the HA-CA hydrogels (Fig. 4d), indicating metabolic switching to glycolysis as the dominant energy-producing pathway in the cartilaginous organoids in the HA-TP hydrogel. Furthermore, the cartilaginous organoids in the HA-TP hydrogels showed significantly lower expression of markers involved in oxidative phosphorylation

https://doi.org/10.1038/s41467-025-57779-6

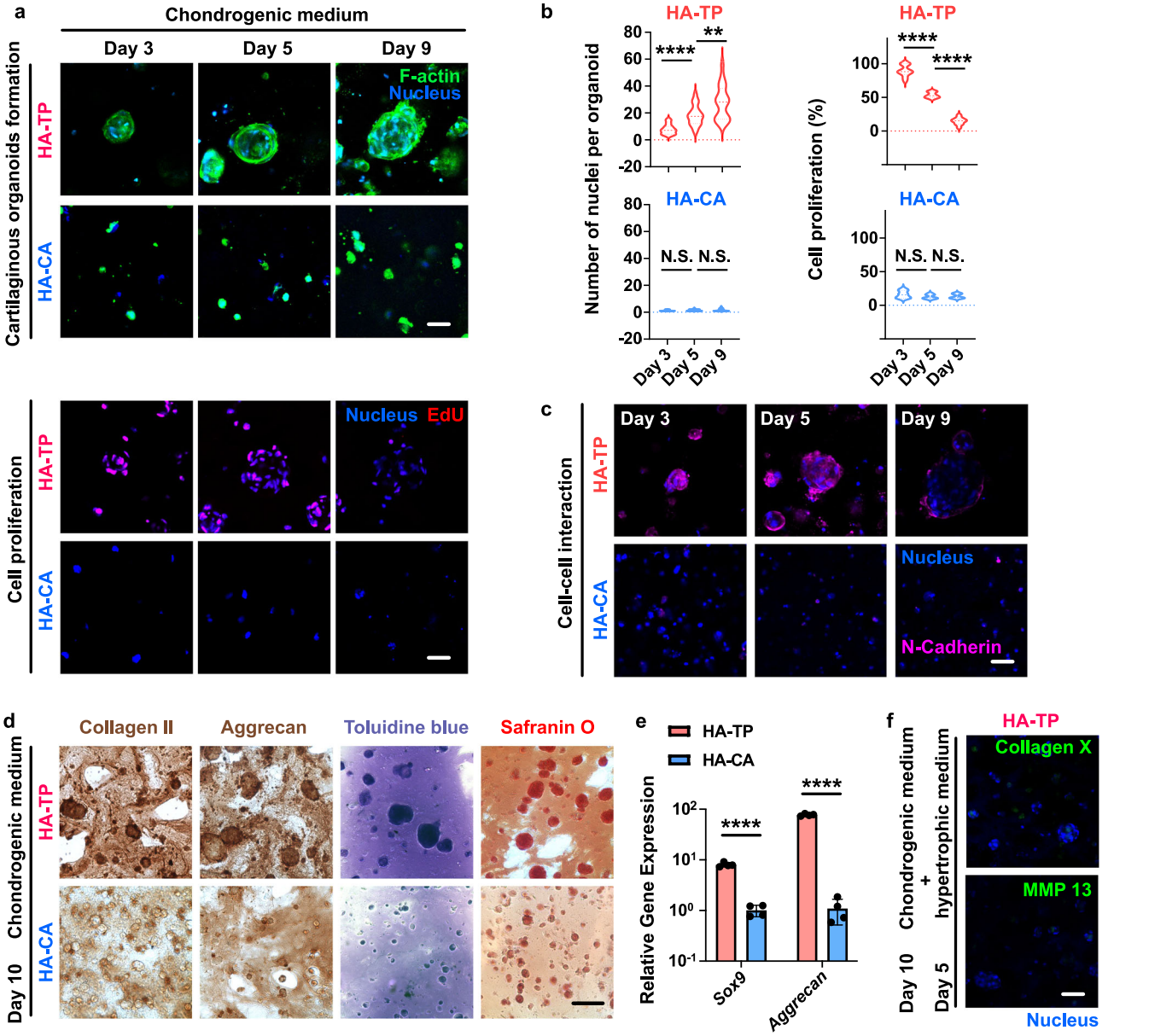

Fig. 3 | The hydrogel with more dynamic crosslinks enhances the formation of cartilaginous organoids, N-cadherin-mediated cell-cell interactions and chondrogenesis and inhibits the hypertrophy of encapsulated organoids. **a** Representative image of hMSCs encapsulated in hydrogels from different groups (HA−TP and HA−CA) on culture days 3, 5, and 9, with staining of F-actin (green), nuclei (blue), and EdU (red). Scale bar: 50 μm. **b** The size of cartilaginous organoids and cell proliferation calculated by EdU staining of encapsulated hMSCs in the hydrogels at different time points (Days 3, 5, and 9). (Number of nuclei per organoid, $n = 12$ organoids per group from 2 independent hydrogels. Cell proliferation, $n = 10$ organoids per group from 2 independent hydrogels. $^{**}p < 0.01$, $^{****}p < 0.0001$, N.S. indicates no significant difference, two-tailed Student's *t*-test) **c** The more dynamic HA-TP hydrogel promotes N-cadherin-mediated cell-cell interactions by supporting the formation of multicellular cartilaginous organoids. Scale bar: 50 μm. **d** Representative images of Toluidine Blue, Safranin O, type II collagen, and aggrecan immunohistochemical staining of the cell-seeded HA-TP and HA-CA hydrogels. Scale bar: 100 μm. **e** The quantification of *Sox9* and *Aggrecan* gene expression by qPCR after 7 days of chondrogenic culture. Values were normalized to the expression levels of the HA-CA group. Data are presented as mean values ± SD, $n = 4$ independent hydrogels; $^{****}p < 0.0001$ (two-tailed Student's *t*-test). **f** Representative images of type X collagen (green) and MMP 13 (green) immunofluorescence staining of the cell-seeded HA-TP hydrogels. Scale bar: 100 μm.

(Succinate dehydrogenase complex, subunit A (*SDHA*), ATP synthase F1 subunit beta (*ATP5FB*) and NADH dehydrogenase 1 (*ND 1*)) than did those single cells in the HA-CA hydrogel (Fig. 4d)[38]. These findings together demonstrate that the highly dynamic HA-TP hydrogel promotes the metabolic switching of encapsulated hMSCs to a state resembling that of native chondrocytes in articular cartilage by enabling the formation of organoids and the associated hypoxic microenvironment, thereby promoting the development of cartilaginous organoids.

Cartilaginous organoids formed in the ultra-dynamic hydrogel reveals the key role of hypoxia-induced histone lactylation in enhancing chondrogenesis

Previous studies have demonstrated that lactate-induced lactylation of histone lysine residues serves as a critical epigenetic mechanism to regulate gene transcription[39]. Our results showed that the cartilaginous organoids in the HA-TP hydrogels produced and accumulated significantly more lactate during 7 days of chondrogenic culture than the single cells in the HA-CA hydrogels (Fig. 5a)[40]. By using the Lactate

https://doi.org/10.1038/s41467-025-57779-6

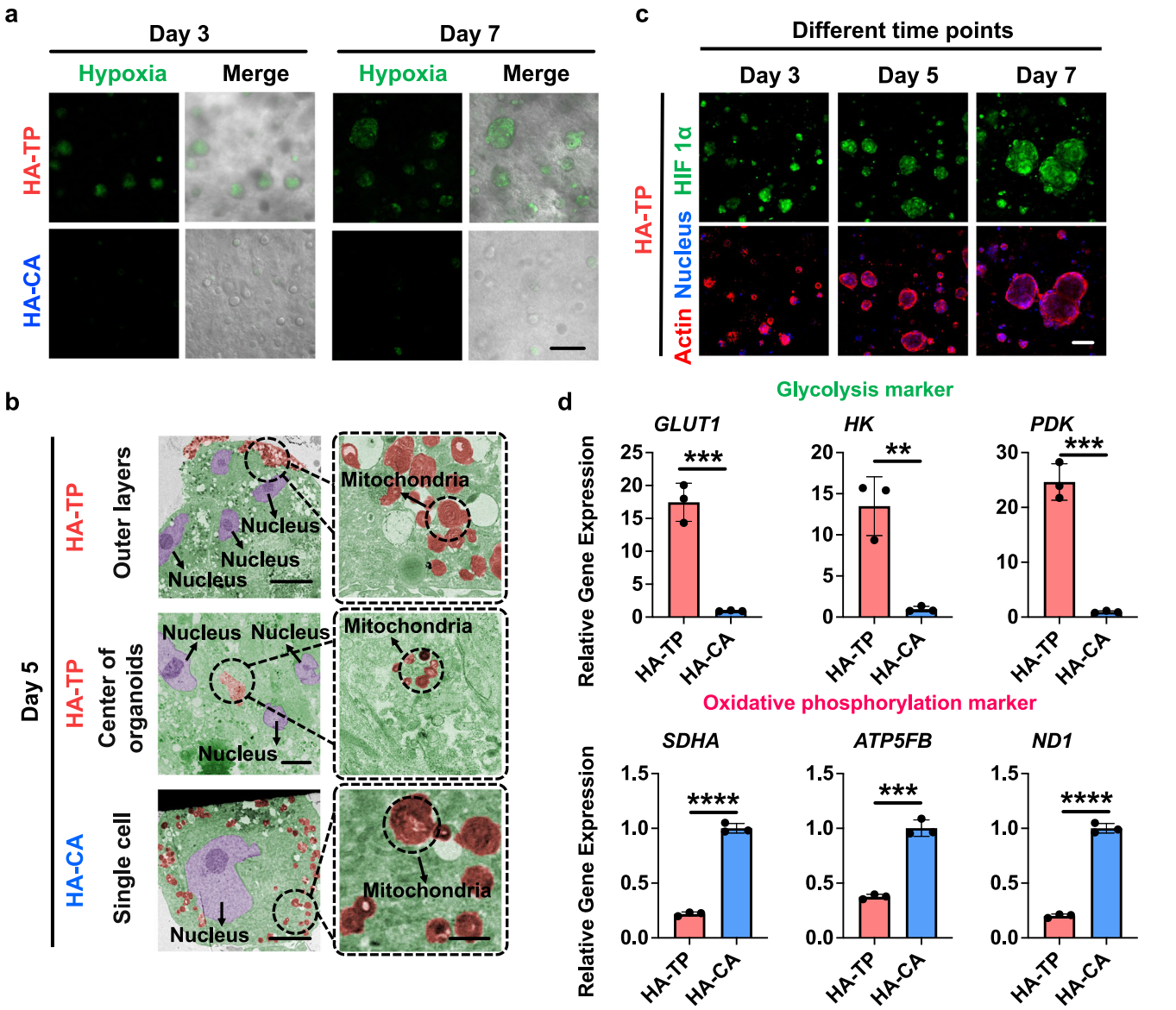

Fig. 4 | The hydrogel with higher network dynamics promotes cell organoid-induced hypoxia and drives a metabolic switch that is favorable for chondrogenesis. a Image-iT green hypoxia staining of hMSCs cultured in the HA-TP and HA-CA hydrogels on Days 3 and 7 of chondrogenic culture. Scale bar: 100 μm. **b** Representative transmission electron microscopy images of hMSCs encapsulated in the HA-TP and HA-CA hydrogels after 5 days of chondrogenic culture. Scale bar: left column, 5 μm; right column, 1 μm. **c** Representative images of immunofluorescence staining of HIF-1α (green), Actin (red), and the nucleus (blue) in encapsulated hMSCs in the HA-TP hydrogel after 3, 5, and 7 days of chondrogenic culture. Scale bar: 100 μm. **d** The expression levels of marker genes related to glycolysis and oxidative phosphorylation quantified by qPCR after 3 days of chondrogenic culture. Values were normalized to the expression levels of the HA-CA group. Data are presented as mean values ± SD, $n = 3$ independent hydrogels, $^{**}p < 0.01$, $^{***}p < 0.001$, $^{****}p < 0.0001$ (two-tailed Student's t-test).

Dehydrogenase Activity Assay Kit, we also found that the cartilaginous organoids in the HA-TP hydrogel had significantly higher lactate dehydrogenase (LDH) activity than the single cells that failed to form organoids in the HA-CA hydrogel (Fig. 5a)[41]. Consistent with these results, the expression levels of lactate dehydrogenase-related marker genes (*LDHA*, *LDHB*) and hypoxia-related marker genes (*MCT2*, *MCT4*) were also upregulated in the cartilaginous organoids in the HA-TP hydrogel (Fig. 5b). These findings suggest that the hypoxic microenvironment resulting from cartilaginous organoids formation due to higher network dynamics in the HA-TP hydrogels enhances lactate dehydrogenase activity and lactate production.

Previous studies have shown that endogenous lactate production is a key determinant of histone lysine lactylation levels[39]. To examine overall lysine lactylation of histones (Kla) of cartilaginous organoids in the HA-TP hydrogel, we first used immunofluorescence staining based on a pan-anti-Kla antibody. The results showed that the histone Kla level in the cartilaginous organoids in the HA-TP hydrogel was significantly higher than that in the single hMSCs in the HA-CA hydrogel (Supplementary Fig. 12). Previous studies have established that lactylation on Lysine 18 of Histone H3 (H3K18la) plays a crucial role in the regulation of gene expression[39,42]. The immunofluorescence staining results based on the H3K18la-specific antibody showed a significantly higher H3K18la modification level in the cartilaginous organoids in the HA-TP hydrogel than in those single cells in the HA-CA hydrogel (Fig. 5c). The in vivo environment has a significant impact on the chondrogenic differentiation of cells, so it is essential to evaluate the histone lactylation of hMSCs in vivo. The subcutaneous implantation experiment in nude mice was utilized to explore the fundamental ability of the HA-TP hydrogel to induce MSC clustering and histone lactylation under a non-hostile in vivo environment. This provides

https://doi.org/10.1038/s41467-025-57779-6

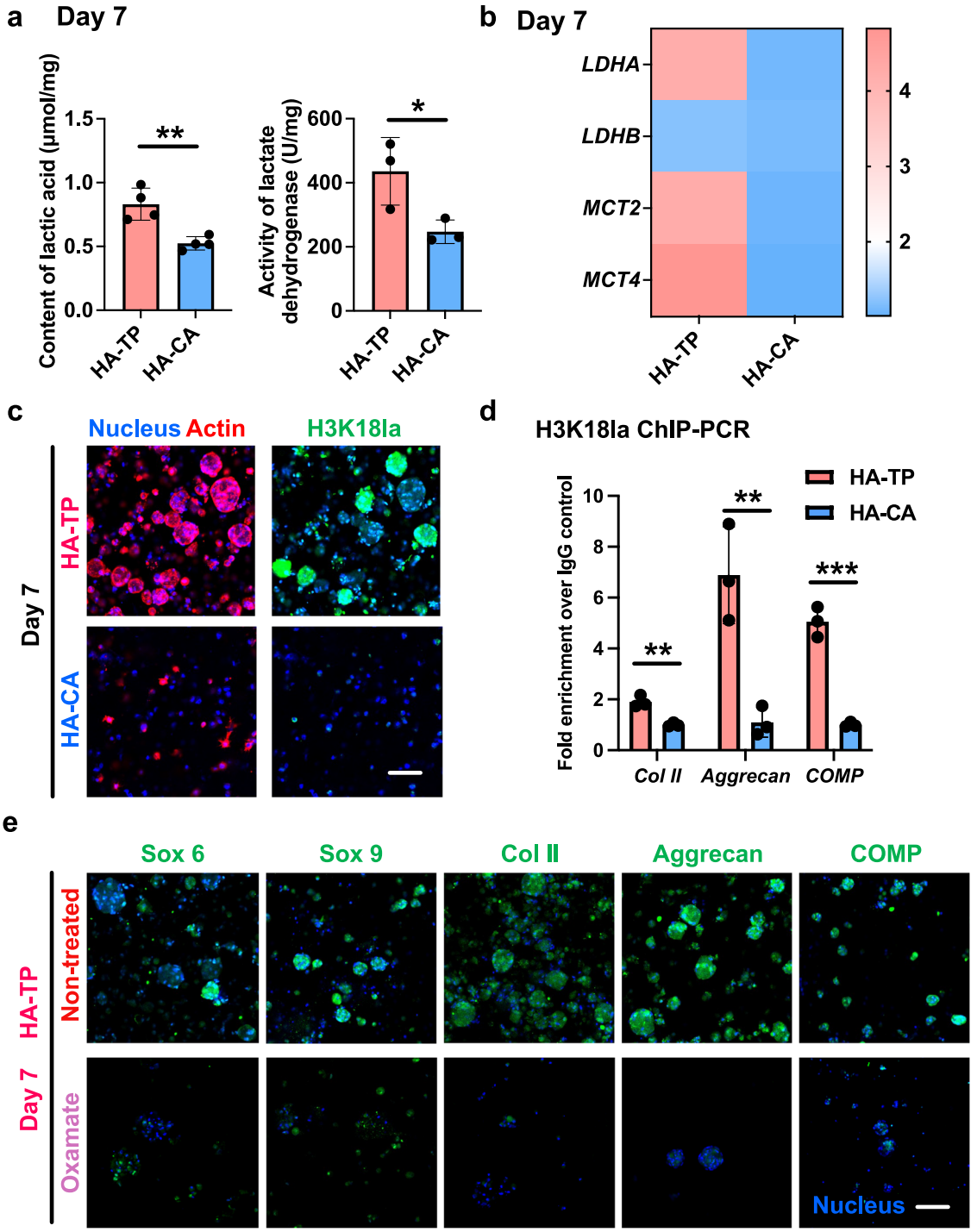

Fig. 5 | Cartilaginous organoids formed in the ultra-dynamic hydrogel reveals the key role of hypoxia-induced histone lactylation in enhancing chondrogenesis. a The cartilaginous organoids formed in the HA-TP hydrogel produced more lactate and had higher lactate dehydrogenase (LDH) activity than the single hMSCs in the HA-CA hydrogel during 7 days of chondrogenic culture. Data are presented as mean values ± SD, $n = 4$ independent hydrogels (content of lactic acid), $n = 3$ independent hydrogels (activity of lactate dehydrogenase). $^{*}p < 0.05$, $^{**}p < 0.01$ (two-tailed Student's t-test). **b** The expression levels of marker genes related to lactate dehydrogenase (*LDHA*, *LDHB*) and hypoxia (*MCT2*, *MCT4*) quantified by qPCR after 7 days of chondrogenic culture. Values were normalized to the expression levels of the HA-CA group, $n = 3$ independent hydrogels. **c** Representative images of immunofluorescence staining of H3K18la (green), Actin (red), and the nucleus (blue) in cartilaginous organoids formed in the HA-TP hydrogel and single hMSCs in the HA-CA hydrogel after 7 days of chondrogenic culture. Scale bar: 100 μm. **d** H3K18la ChIP–qPCR results of cartilaginous organoids formed in the HA-TP or single hMSCs in the HA-CA hydrogels after 7 days of chondrogenic culture. Data are presented as mean values ± SD, $n = 3$ independent hydrogels. $^{**}p < 0.01$, $^{***}p < 0.001$ (two-tailed Student's t-test). **e** Immunofluorescence staining of chondrogenic transcription factors (Sox6 and Sox9), Collagen II, Aggrecan, and COMP in cartilaginous organoids formed in the HA–TP hydrogels after 7 days of chondrogenic culture with or without treatment with lactate dehydrogenase inhibitors. Scale bar = 100 μm.

proof-of-concept evidence for the hydrogel's ability to promote lactylation-driven epigenetic modifications. In the subcutaneous implantation experiment in nude mice, we studied the fate of cells loaded in hydrogels after implantation. Immunofluorescence staining revealed that hMSCs encapsulated in the HA-TP hydrogel implanted in subcutaneous pockets of nude mice formed large cartilaginous organoids and exhibited significant expression of H3K18la. In contrast, hMSCs within the implanted HA-CA hydrogel remained as individual cells with low H3K18la expression (Supplementary Figs. 13 and 14). The upregulation of H3K18la within the cartilage organoids formed in the ultra-dynamic hydrogel suggests a positive correlation between histone lactylation and chondrogenesis.

To study the correlations between H3K18la modification and chondrogenesis-related gene expression, we performed chromatin immunoprecipitation followed by quantitative PCR (ChIP–qPCR) using the anti-H3K18la antibody. The ChIP–qPCR results demonstrated that H3K18la was significantly more enriched specifically in the promoter regions of chondrogenesis genes (*Aggrecan*, *Collagen II* and *COMP*) in the cartilaginous organoids in the HA-TP hydrogel than in the single hMSCs in the HA-CA hydrogel (Supplementary Fig. 15, Fig. 5d). Previous studies showed that lactate dehydrogenase inhibitors attenuated lactate production and histone lactylation under hypoxia[43]. To examine the impact of histone lactylation on the expression of chondrogenic transcription factors and cartilaginous ECM components, the hMSC-laden HA-TP hydrogels were treated with pharmacological inhibitors targeting both LDHA and LDHB[43]. The untreated control HA-TP hydrogel showed robust expression and nuclear localization of chondrogenic transcription factors (Sox5, Sox6, and Sox9) as well as substantial cartilaginous matrix deposition (Col II, Aggrecan, and COMP) in hMSC-derived cartilaginous organoids after 7 days of culture (Fig. 5e and Supplementary Fig. 16)[44,45]. In contrast, although the hMSCs in the HA-TP hydrogel treated with LDHA and LDHB inhibitors (oxamate) could still form cell aggregates, the expression of chondrogenic transcription factors and cartilaginous matrix deposition within these aggregates were significantly decreased (Fig. 5e and Supplementary Fig. 17), demonstrating the indispensable role of lactate in mediating the formation of cartilaginous organoids from hMSCs. The organoids encapsulated in the HA-TP hydrogel containing the inhibitor of p300, a potential histone lactylation catalyst, showed significantly lower expression of type II collagen (Col II) after 7 days of induction in chondrogenic medium compared to the organoids encapsulated in the HA-TP hydrogel without the inhibitor (Supplementary Fig. 17). Additionally, the expression of type II collagen was significantly increased in organoids in the HA-TP hydrogel treated with the medium supplement of 5 mM sodium lactate (Supplementary Fig. 17). These findings together indicate that the dynamic HA-TP hydrogel facilitates the development of hMSC spheroids and a hypoxic microenvironment, which induces metabolic switching and lactate accumulation to enhance histone lactylation, which in turn promotes formation of cartilaginous organoids (Fig. 1).

Histone lactylation promotes formation of cartilaginous organoids by regulating transcriptional accessibility of chondrogenic genes

We hypothesize that histone lactylation can enhance the transcriptional accessibility of chondrogenic genes similar to many other histone epigenetic modifications[42]. To verify this hypothesis, we performed chromatin immunoprecipitation (ChIP) using anti-H3K18 lactylation antibodies on the cartilaginous organoids facilitated by the dynamic hydrogel, followed by sequencing (ChIP-seq) (Fig. 6a). The ChIP-seq data revealed that histone lactylation modifications were highly enriched in the promoter regions, accounting for 33.29% of the total peaks (Fig. 6b). Cartilaginous organoids of the HA-TP group showed a total of 7456 differential genes associated with lactylation modification sites compared with isolated cells of the HA-CA group. Among these genes, there were 1001 significantly upregulated genes (twofold increase) and 332 significantly downregulated genes (twofold decrease) specifically associated with lactylation modification sites (Fig. 6c). Furthermore, the upregulated genes associated with lactylation modification in the HA-TP group included the classic chondrogenic transcription factors (*Sox5*, *Sox6*, and *EBF1*[46]) (Fig. 6d, e and supplementary Fig. 18). The ChIP-seq results also revealed that the promoter region of *HIF-1α* is located within the gene sequences associated with lactylation-modified histones (Fig. 6d, e). This finding suggests that the histone lactylation induced by the hypoxic metabolite can promote the expression of HIF-1α in return. Furthermore, the ChIP-seq results also revealed that the upregulated genes associated with lactylation modification in the HA-TP group included the promoters of genes related to cartilaginous matrix components (*HAPLN1*[47], *CRTAP*, and *ACAN*) and chondrogenic growth factors (*TGFB2*[48], *TGFBI*[49], and *GDF5*[50]) (Fig. 6d–f). In contrast, ChIP-seq results showed the downregulation of all these genes in HA-CA hydrogels, which can be attributed to the low level of histone lactylation modification of HA-CA group. Gene Ontology (GO) analysis revealed that these lactylation-specific genes were enriched in biological functions related to the responses to low oxygen conditions, biosynthesis of cartilaginous matrix, chondrogenic secretory factors (*TGFβ* and *IGF*), chondrocyte proliferation and differentiation, and cartilage development (Fig. 6g, Supplementary Fig. 19). In fact, histone acylations (such as acetylation, crotonylation, and lactylation) have been shown to directly increase transcription efficiency in cell-free systems[42]. These findings indicate that the enhanced histone lactylation in the cell spheroids in HA-TP hydrogel can potentially increase the transcriptional accessibility of genes associated with key chondrogenesis processes, thereby facilitating the formation of cartilaginous organoids by the encapsulated hMSCs.

Cartilaginous organoids formed in ultra-dynamic hydrogel promotes cartilage repair in osteochondral defects

To further evaluate the efficacy of cartilaginous organoids generated in the hydrogels to repair cartilage defects, the HA-TP and HA-CA hydrogels encapsulating rat MSCs (rMSCs) were first cultured in chondrogenic medium for 5 days to induce cartilage organoid formation, and then implanted into osteochondral defects in rat knees (Fig. 7a)[6,51]. At 6 weeks after implantation, macroscopic views revealed fully regenerated white and smooth neocartilage well integrated with the surrounding tissue in all the defects treated with the HA-TP hydrogel, closely resembling the healthy control (Fig. 7b). In contrast, partial cartilage defects were still clearly visible in the center of the defects treated with the HA-CA hydrogel, and the circular defect boundary with the surrounding host cartilage was easily distinguishable (Fig. 7b). Immunobiological stainings further revealed increased deposition of cartilage-specific type II collagen and reduced presence of type I collagen (fibrocartilage marker) and MMP-13 (hypertrophy marker) in the HA-TP group compared with that in the HA-CA group (Fig. 7c, Supplementary Figs. 20, 21). The histological Wakitani score of the HA-TP group was markedly lower than that of the HA-CA group (Fig. 7d). These findings indicated that the ultra-dyanmic HA-TP hydrogel can promote chondrogenesis of the encapsulated rMSCs and enhance hyaline neocartilage regeneration in a rat osteochondral defect model. It should be noted that in contrast to the disorganized osteochondral structure in the HA-CA hydrogel group, treatment with the HA-TP hydrogel regenerated a distinct chondral layer on top of the regenerated subchondral bone with a clear osteochondral interface (Fig. 7c). To further examine the details of hydrogel-mediated subchondral bone repair, freeze-dried HA-TP and HA-CA hydrogel sponges were implanted in the rat distal femoral bone defects (Fig. 7e). At 4 weeks after implantation, the Safranin O and Methylene Blue stainings reveal both abundant formation of neocartilage and the

https://doi.org/10.1038/s41467-025-57779-6

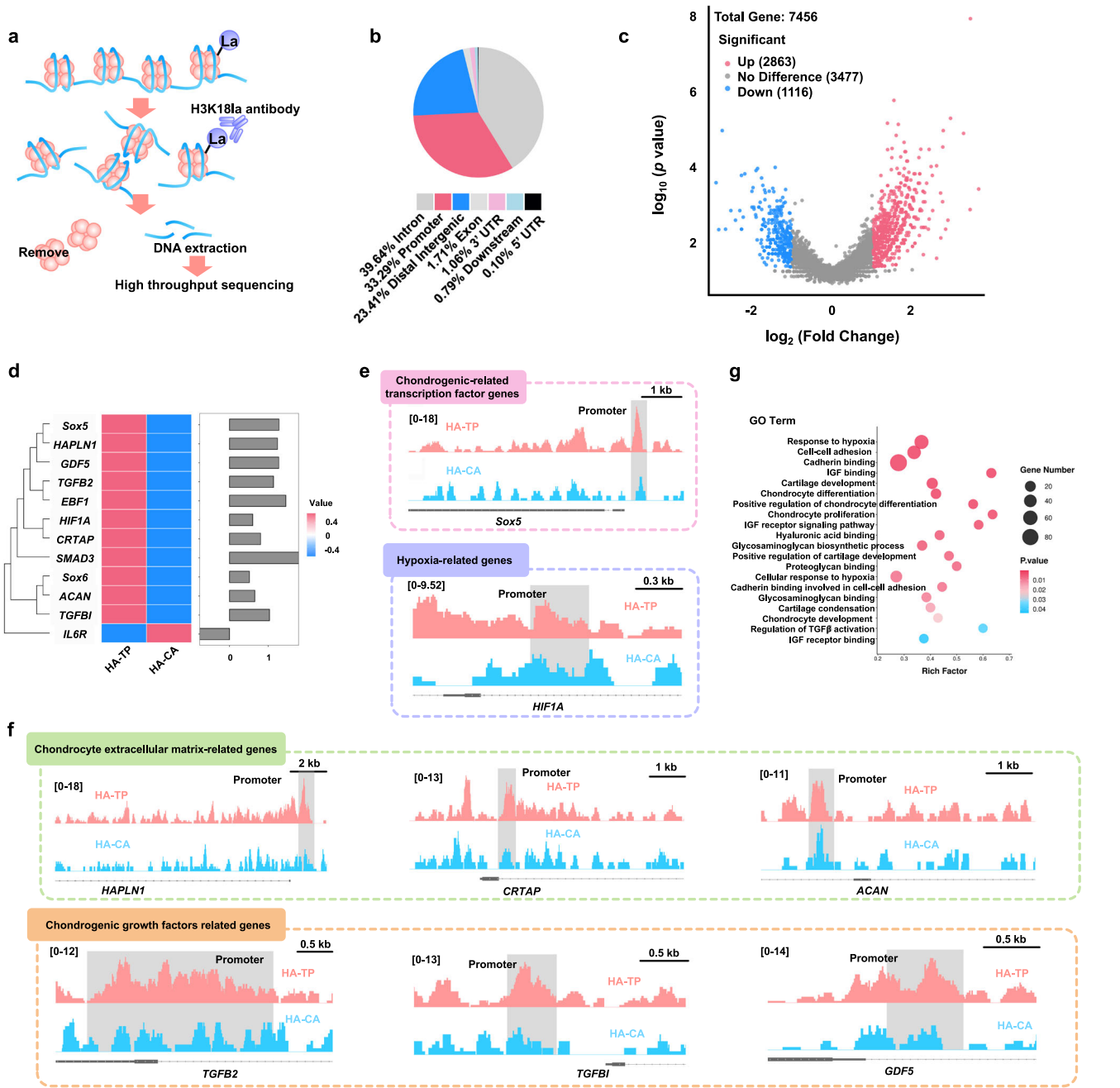

Fig. 6 | Histone lactylation is enriched in the promoters of genes associated with chondrogenic differentiation. a Schematic diagram of the principle of H3K18la chromatin immunoprecipitation sequencing (ChIP-seq). **b** Pie chart showing the genomic distribution of H3K18la peaks. **c** Volcano plot of genes associated with lactylation peaks from cells encapsulated in HA-TP and HA-CA hydrogels. The significantly upregulated and downregulated genes are labeled in pink and blue, respectively (p value < 0.05, MAnorm). **d** Heat maps showing fold change (FC) in the expression level of chonrogenic genes in HA-TP vs. HA-CA group. **e**, **f** Genome browser tracks showing HA-TP and HA-CA ChIP-seq peaks at the promoters of genes related to chondrogenic transcription factor (*Sox5*), hypoxia (*HIF1A*), cartilaginous matrix (*HAPLN1*, *CRTAP* and *ACAN*), and chondrogenic growth factor (*TGFB2*, *TGFBI* and *GDF5*). **g** Dot plot displaying the gene ontology (GO) enrichment analysis of genes in the differential ChIP-seq peaks between the HA-TP and HA-CA group. The size of bubble represents the number of differential genes enriched in each GO term.

interspersed putative osteoblasts (deep blue) and osteoid tissue (purple-gray) in the HA-TP treatment group, indicating the ongoing endochondral ossification process, which was not found in the HA-CA group (Fig. 7f). These findings suggest that acellular HA-TP hydrogel implanted in the subchondral bone can recruit host bone marrow cells to first initiate formation of cartilaginous organoids and then the subsequent endochondral ossification. Such tissue-adaptable nature of the ultra-dynamic hydrogel enables its potential application to facilitate the repair of complex tissues.

Acellular ultra-dynamic hydrogel expedites porcine cartilage repair by enhancing histone lactylation of recuited cells

To further validate the efficacy of acellular HA-TP hydrogel to repair cartilage defects through recruiting endogenous cells to form cartilaginous organoids and promoting histone lactylation, we implanted the lyophilized HA-TP and HA-CA hydrogel sponges into swine knee cartilage defects (Fig. 8a and Supplementary Fig. 22a). After 8 weeks of implantation, the cartilage defect sites in the HA-TP group showed a smooth articular surface with similar color as that of the surrounding

https://doi.org/10.1038/s41467-025-57779-6

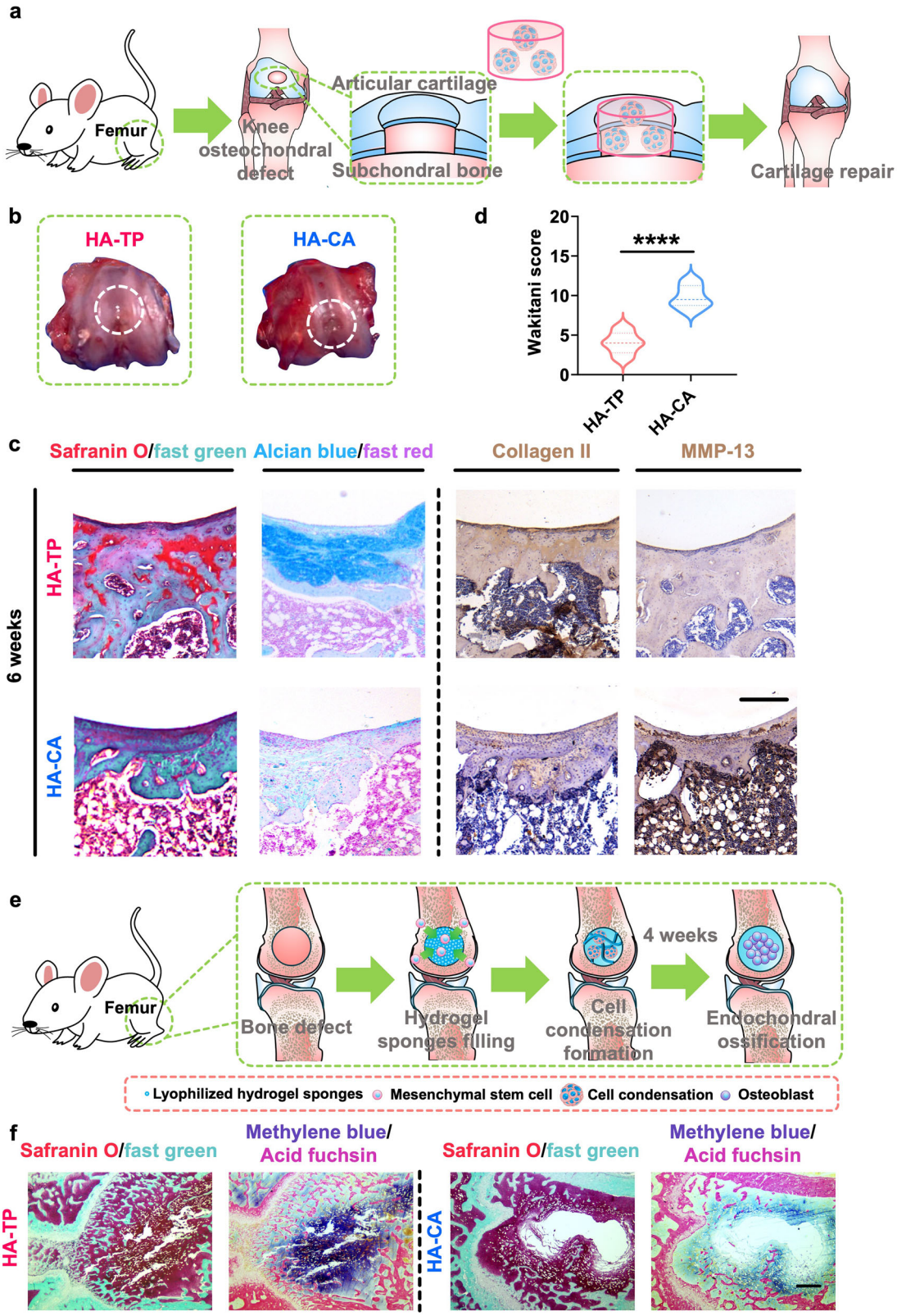

Fig. 7 | The cartilaginous organoids induced by higher network dynamics substantially enhances the in situ regeneration of hyaline cartilage and subchondral bone in rat osteochondral defects. a Schematic illustration of the implantation of rMSC-laden hydrogels in rat osteochondral defects. **b** Macroscopic views of articular cartilage defects treated with cell-laden HA-TP and HA-CA hydrogels at 6 weeks after implantation. **c** Safranin O and Alcian blue staining for glycosaminoglycans and immunohistochemical staining (Collagen II and MMP-13) of the tissue in articular cartilage defects treated with HA-TP and HA-CA hydrogels at 6 weeks after implantation. Scale bar = 150 μm. **d** Histological scoring of in vivo samples showing significantly lower scores for the HA-TP hydrogel treatment group, $n = 3$ independent sections from different tissues, $^{****}p < 0.0001$ (two-tailed Student's t-test). **e** Schematic illustration of the implantation of rMSC-free lyophilized hydrogels in rat bone defects. **f** Safranin O/Fast green staining for glycosaminoglycans and Methylene blue/Acid fuchsin staining of the tissue in bone defects treated with HA-TP and HA-CA hydrogels at 4 weeks after implantation. Scale bar = 100 μm.

https://doi.org/10.1038/s41467-025-57779-6

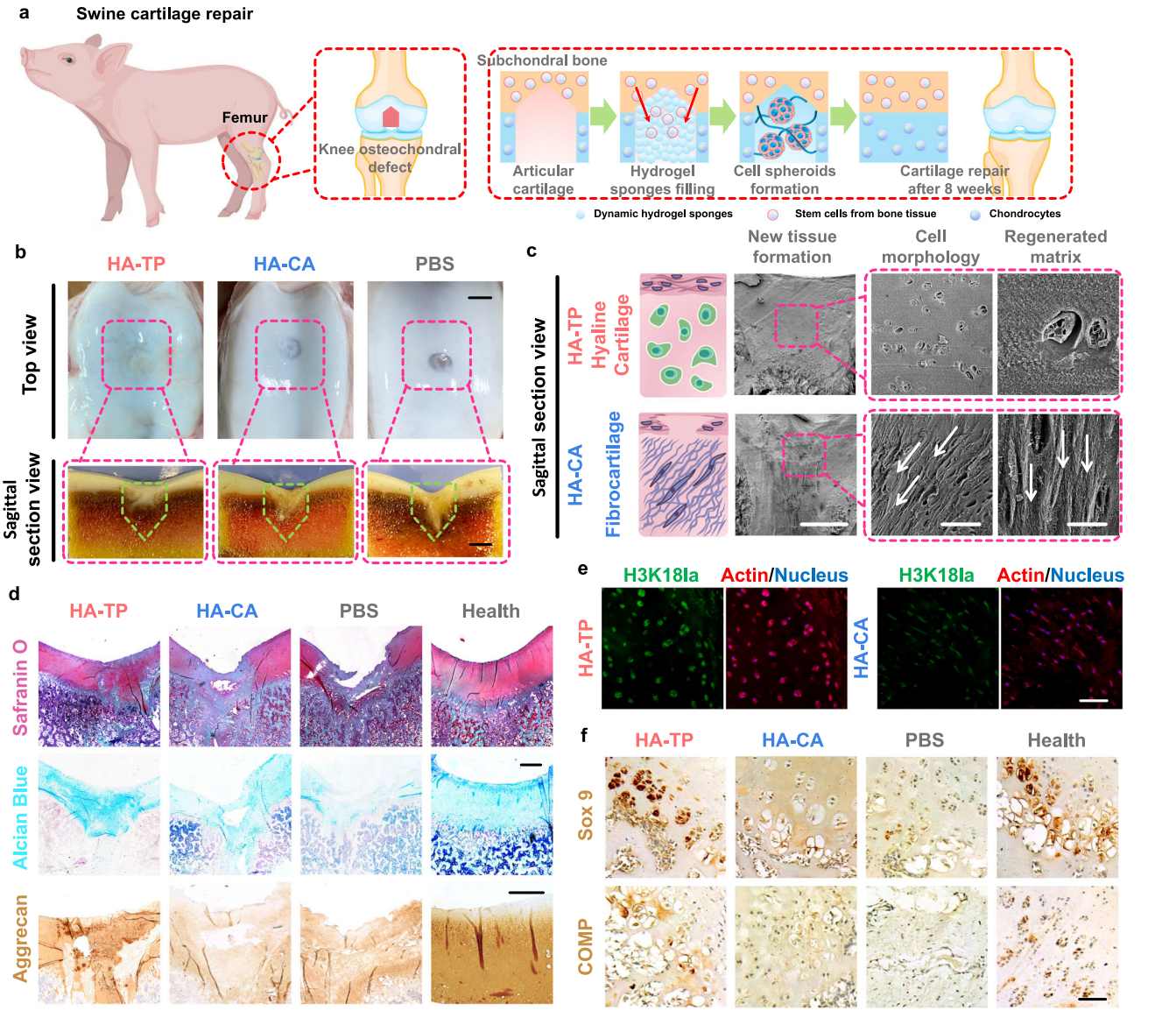

Fig. 8 | The cell-free ultra-dynamic hydrogel substantially enhances the in situ regeneration of hyaline cartilage and subchondral bone in swine osteochondral defects. a Schematic illustration of the implantation of free-dried acellular hydrogel sponges in swine osteochondral defects. **b** Macroscopic views of the top and longitudinal section of articular cartilage defects treated with acellular HA-TP and HA-CA hydrogels at 8 weeks after implantation. Scale bar: Top view, 5 mm; Sagittal section view, 2 mm. **c** SEM images of the saggital sections of articular cartilage defects treated with acellular HA-TP and HA-CA hydrogels at 8 weeks after implantation. Scale bar: second column, 1 mm; third column, 50 μm; fourth column, 10 μm. **d** Safranin O and Alcian Blue staining (scale bar = 1 mm) and immunohistochemical staining (Aggrecan, scale bar = 100 μm) images of articular cartilage defects treated with HA-TP and HA-CA hydrogels and PBS at 8 weeks after implantation, and healthy cartilage tissue. **e** Images of immunofluorescence staining against H3K18la (scale bar = 50 μm) for articular cartilage defects at 8 weeks after treatment with HA-TP and HA-CA hydrogels. **f** Images of immunohistochemical staining (Sox9 and COMP, scale bar = 50 μm) of articular cartilage defects treated with HA-TP, HA-CA hydrogels, and PBS, as well as healthy cartilage tissue. Scale bar: 50 μm. Some components of (**a**) were created in BioRender. boguang, y. (2025) https://BioRender.com/ b24y218.

healthy tissue (Fig. 8b and Supplementary Figs. 23, 24). In contrast, the HA-CA group only showed partial repair with significant remaining defects, while the PBS treatment group also exhibited limited repair with exposed subchondral bone in the defect site (Fig. 8b and Supplementary Figs. 23, 24). The tissue sections cut perpendicular to the articular surface showed that the subchondral bone in the HA-TP group was well repaired. In contrast, the HA-CA group exhibited partial repair of the subchondral bone defects partilly filled with white fibrotic tissue, while the PBS group showed no repair of the subchondral bone defects, which were entirely filled with white fibrotic tissue (Fig. 8b and Supplementary Fig. 23). Scanning electron microscopy results revealed that the distinct structures and distribution of recruited endogenous cells in the newly formed tissue of the HA-TP group compared with that of control groups. Similar to that observed in the healthy hyaline cartilage, the recuited cells in the newly formed tissue of the HA-TP group displayed the rounded chondrocyte morphology and were randomly dispersed in the isotropic extracellular matrices consisting of dense proteoglycan and collagen fibers of isotropic arrangement (Fig. 8c). In contrast, the defects in the HA-CA and PBS contained excessive anisotropically arranged collagen fibers, and the cells were distributed in alignment with the collagen fibers, indicating the formation of fibrocartilage instead of the functional hyaline cartilage (Fig. 8c and Supplementary Fig. 23). The Safranin O and Alcian Blue staining showed higher staining intensity against cartilaginous matrix components, including sulfated glycosaminoglycans in the HA-TP hydrogel treatment group compared with that of the HA-CA and

PBS groups (Fig. 8d). The same trend was observed in the immunohistochemical staining of Aggrecan (Fig. 8d). Lubricin is a proteoglycan found in synovial fluid and on the surface of articular cartilage (superficial layer), playing a crucial role in joint lubrication and synovial homeostasis[52]. We performed immunofluorescence staining for lubricin in sections of the newly formed tissues from pig cartilage repairs. The staining results revealed the expression of lubricin in the articular surface layer of the regenerated cartilage from the dynamic HA-TP hydrogel treatment group. In contrast, the HA-CA hydrogel treatment group and the PBS control groups displayed no detectable lubricin expression (Supplementary Fig. 25).

Immunofluorescence staining of H3K18la revealed high expression and nuclear localization of H3K18la in the HA-TP group exhibited, similar to that of healthy cartilage (Fig. 8e), whereas the expression and nuclear localization of H3K18la were minimal in the elongated fibroblast-like cells found in the defects of the HA-CA group and PBS group (Supplementary Fig. 26). Immunohistochemical staining also revealed significantly higher nuclear expression of Sox 9, a key chondrogenic transcription factor, and matrix presence of cartilage oligomeric matrix protein (COMP), critical to collagen assembly and stability, in the HA-TP group compared with that in the HA-CA and PBS groups (Fig. 8f). These results collectively demonstrate that the implanted acellular HA-TP hydrogel can effectively promote the histone lactylation (H3K18la) in the recruited endogenous cells at cartilage defects, thereby facilitating the chondrogenesis and expediting the regeneratin of hyaline cartilage within 2 months (typically requires 6 months) in the large animal model. The capability of HA-TP hydrogel alone to promote cartilage regeneration without the encapsulated cells also simplifies the regulatory approval process for clinical translation.

In this work, we fabricated an ultra-dyanmic hydrogel (HA-TP) by employing a host–guest complexation with high dissociation kinetics. Compared to a hydrogel with low network dynamics, the ultra-dynamic hydrogel promoted the formation of cartilaginous organoids, enhanced cell-cell interactions, and established a hypoxic microenvironment within the cartilaginous organoids, which induced the metabolic reprogramming of hMSCs towards glycolysis, resembling the process of cartilage development. We further showed that the enhanced hypoxic metabolism resulted in the elevated histone lactylation, leading to the enhanced formation of cartilaginous organoids. Our ChIP-seq results further highlighted the critical role of histone lactylation in regulating gene expression during the process of cartilaginous organoid differentiation. Our in vivo data demonstrated that the ultra-dynamic hydrogel network that promotes the formation of cartilaginous organoids enhanced the regeneration of hyaline cartilage and subchondral bone in a rat osteochondral defect model. Furthermore, in a porcine cartilage defect model, the implantation of lyophilized cell-free ultra-dynamic hydrogel sponge promoted the histone lactylation of recruited endogenous cells to expedite the regeneration of hyaline cartilage in 2 months. Our dynamic supramolecular hydrogel with defined chemical composition provides a tuneable platform to assist not only fundamental investigations of cellular development and associated metabolic reprogramming in a 3D microenvironment but also translational studies to develop effective delivery vehicles for therapeutic cells.

Methods

Acrylated β-cyclodextrin (Ac-β-CD) preparation

β-Cyclodextrin (6.6 g) and (triethyl)amine (4.6 mL) were dissolved in 100 mL DMF solvent. The resulting solution was stirred at 0 °C, and 3.3 ml of acryloyl chloride was added dropwise into the reaction mixture. The reaction mixture was stirred for 12 h. After that, the reaction mixture was filtered to remove the byproduct, and the obtained crude Ac-β-CD solution was concentrated under reduced pressure. Then, the solution was dropped into cold acetone, and the white precipitate of modified β-CD was obtained after filtration.

HA-TP and HA-CA preparation

Purified tetra butyl-ammonium salt of HA (HA-TBA) (0.5 g, 0.7 mmol disaccharide repeat units) was weighed into a 100 mL Schott flask and dissolved in 35 mL of DMSO solvent. 4-Tert-butylphenylacetic acid (3 eq), dimethyl amino pyridine (DMAP; 0.75 eq) and di-tert-butyl dicarbonate (0.9 eq) were added, and the reaction was stirred for 20 h at 45 °C. The solution was then transferred to a 10 kDa MWCO dialysis tube and dialyzed against DMSO, NaCl solutions, and finally deionized water. A white fluffy solid was obtained after lyophilization.

The synthesis of HA-CA was slightly different from the modification of HA-TP. Because of the greater steric hindrance of cholic acid, di-tert-butyl dicarbonate (1.8 eq) was added to ensure that HA-CA had the same degree of substitution as HA-TP.

Encapsulation of hMSCs in the HA-TP and HA-CA hydrogels

We acquired passage 4 normal human bone marrow-derived mesenchymal stem cells (hMSCs) (Lonza, Allendale, New Jersey, USA, Catalog #: PT-2501, Lot #: 19TL329433, from male) expanded in growth medium (α-MEM supplemented with 16.7% FBS, 1% penicillin/streptomycin, and 1% L-glutamine) (Thermo Fisher Scientific, Waltham, Massachusetts, USA). The cell pellet was mixed with the HA-TP and HA-CA precursors to obtain a cell suspension at a concentration of 10 million cells mL^{-1}. The 50 μL mixture was transferred into a PDMS mold with a diameter of 4 mm and placed under UV light for 10 min of gelation. All hydrogels were supplemented with 2 mL of chondrogenic medium (DMEM, 1% ITS + Premix, 1% penicillin/streptomycin, 50 μg/mL L-proline, 1 mM sodium pyruvate, 50 μg/mL L-ascorbic acid-2-phosphate, 100 nM dexamethasone, and 10 ng/mL TGF-β_1), and the medium was replaced every 24 h. Samples were collected at specific time points to assess the cell morphology and metabolic pathways of the cells.

Image-iT™ Green Hypoxia Reagent staining

For hypoxia staining, cells encapsulated in the HA-TP and HA-CA hydrogels were cultured in chondrogenic medium for 3 and 7 days before staining with Image-iT Green Hypoxia Reagent (Thermo Fisher Scientific) according to the manufacturer's recommendations. Fluorescence images were acquired with a Nikon C2 + confocal microscope using the brightfield and green fluorescence channels and analyzed using ImageJ.

Statistics and reproducibility

GraphPad Prism 10 software was used for all statistical analyses. The data are presented as the mean ± standard deviation. The statistical analysis was performed using two-tailed Student's *t*-tests (for two experimental groups). In the Figs. 3f, 7c, f, and 8c–f, each experiment was repeated three times independently.

Reporting summary

Further information on research design is available in the Nature Portfolio Reporting Summary linked to this article.

Data availability

The data supporting the findings from this study are available within the Article, Supplementary Information, or Source Data file. Source data are provided with this paper. Source data is available for Figs. 2e, 3b, e, 4d, 5a, d, and 6d and Supplementary Figs. 3, 5, 6b, 8, 11, 14, 15, 22b, and 24b in the associated source data file. The raw and processed sequencing data (ChIP-seq) generated in this study have been deposited in the Gene Expression Omnibus (GEO) database under accession number GSE280956. Source data are provided with this paper.

References

1. Rosales, A. M. & Anseth, K. S. The design of reversible hydrogels to capture extracellular matrix dynamics. *Nat. Rev. Mater.* **1**, 15012 (2016).

2. Chaudhuri, O., Cooper-White, J., Janmey, P. A., Mooney, D. J. & Shenoy, V. B. Effects of extracellular matrix viscoelasticity on cellular behaviour. *Nature* **584**, 535–546 (2020).
3. Zhang, K. Y., Feng, Q., Fang, Z. W., Gu, L. & Bian, L. M. Structurally dynamic hydrogels for biomedical applications: pursuing a fine balance between macroscopic stability and microscopic dynamics. *Chem. Rev.* **121**, 11149–11193 (2021).
4. Lee, H. P., Gu, L., Mooney, D. J., Levenston, M. E. & Chaudhuri, O. Mechanical confinement regulates cartilage matrix formation by chondrocytes. *Nat. Mater.* **16**, 1243–1251 (2017).
5. Tan, Y., Huang, H., Ayers, D. C. & Song, J. Modulating viscoelasticity, stiffness, and degradation of synthetic cellular niches via stoichiometric tuning of covalent versus dynamic noncovalent crosslinking. *ACS Cent. Sci.* **4**, 971–981 (2018).
6. Xu, J. B. et al. Injectable stem cell-laden supramolecular hydrogels enhance in situ osteochondral regeneration via the sustained co-delivery of hydrophilic and hydrophobic chondrogenic molecules. *Biomaterials* **210**, 51–61 (2019).
7. Chaudhuri, O. et al. Hydrogels with tunable stress relaxation regulate stem cell fate and activity. *Nat. Mater.* **15**, 326–334 (2016).
8. Yang, B. G. et al. Enhanced mechanosensing of cells in synthetic 3D matrix with controlled biophysical dynamics. *Nat. Commun.* **12**, 3514 (2021).
9. Sasai, Y. Next-generation regenerative medicine: organogenesis from stem cells in 3D culture. *Cell Stem Cell* **12**, 520–530 (2013).
10. Zhang, H. et al. Direct 3D printed biomimetic scaffolds based on hydrogel microparticles for cell spheroid growth. *Adv. Funct. Mater.* **30**, 1910573 (2020).
11. Zhang, K. X., Yan, S. F., Li, G. F., Cui, L. & Yin, J. B. In-situ birth of MSCs multicellular spheroids in poly(L-glutamic acid)/chitosan scaffold for hyaline-like cartilage regeneration. *Biomaterials* **71**, 24–34 (2015).
12. Stocum, D. L. *Regenerative Biology and Medicine* 2nd edn, 1–461 (Elsevier Science, 2012).
13. Richardson, B. M., Wilcox, D. G., Randolph, M. A. & Anseth, K. S. Hydrazone covalent adaptable networks modulate extracellular matrix deposition for cartilage tissue engineering. *Acta Biomater.* **83**, 71–82 (2019).
14. Chaudhuri, O. Viscoelastic hydrogels for 3D cell culture. *Biomater. Sci.* **5**, 1480–1490 (2017).
15. Ma, Y. F. et al. Viscoelastic cell microenvironment: hydrogel-based strategy for recapitulating dynamic ECM mechanics. *Adv. Funct. Mater.* **31**, 2100848 (2021).
16. Krajina, B. A. et al. Dynamic light scattering microrheology reveals multiscale viscoelasticity of polymer gels and precious biological materials. *ACS Cent. Sci.* **3**, 1294–1303 (2017).
17. Liu, W. et al. Probing sol-gel matrices and dynamics of star PEG hydrogels near overlap concentration. *Macromolecules* **52**, 8956–8966 (2019).
18. Kim, I. G., Ko, J., Lee, H. R., Do, S. H. & Park, K. Mesenchymal cells condensation-inducible mesh scaffolds for cartilage tissue engineering. *Biomaterials* **85**, 18–29 (2016).
19. Chameettachal, S., Midha, S. & Ghosh, S. Regulation of chondrogenesis and hypertrophy in silk fibroin-gelatin-based 3D bioprinted constructs. *ACS Biomater. Sci. Eng.* **2**, 1450–1463 (2016).
20. Oberlender, S. A. & Tuan, R. S. Spatiotemporal profile of N-cadherin expression in the developing limb mesenchyme. *Cell Adhes. Commun.* **2**, 521–537 (1994).
21. DeLise, A. M. & Tuan, R. S. Alterations in the spatiotemporal expression pattern and function of N-cadherin inhibit cellular condensation and chondrogenesis of limb mesenchymal cells in vitro. *J. Cell Biochem.* **87**, 342–359 (2002).
22. Zhu, M. L. et al. Hydrogels functionalized with N-cadherin mimetic peptide enhance osteogenesis of hMSCs by emulating the osteogenic niche. *Biomaterials* **77**, 44–52 (2016).
23. Bian, L. M., Guvendiren, M., Mauck, R. L. & Burdick, J. A. Hydrogels that mimic developmentally relevant matrix and N-cadherin interactions enhance MSC chondrogenesis. *Proc. Natl. Acad. Sci. USA* **110**, 10117–10122 (2013).
24. Cosgrove, B. D. et al. N-cadherin adhesive interactions modulate matrix mechanosensing and fate commitment of mesenchymal stem cells. *Nat. Mater.* **15**, 1297–1306 (2016).
25. Murphy, M. P. et al. Articular cartilage regeneration by activated skeletal stem cells. *Nat. Med.* **26**, 1583–1592 (2020).
26. Patel, J. M., Saleh, K. S., Burdick, J. A. & Mauck, R. L. Bioactive factors for cartilage repair and regeneration: improving delivery, retention, and activity. *Acta Biomater.* **93**, 222–238 (2019).
27. Mueller, M. B. & Tuan, R. S. Functional characterization of hypertrophy in chondrogenesis of human mesenchymal stem cells. *Arthritis Rheum.* **58**, 1377–1388 (2008).
28. Paggi, C. A., Teixeira, L. M., Le Gac, S. & Karperien, M. Joint-on-chip platforms: entering a new era of in vitro models for arthritis. *Nat. Rev. Rheumatol.* **18**, 217–231 (2022).
29. Leijten, J. et al. Metabolic programming of mesenchymal stromal cells by oxygen tension directs chondrogenic cell fate. *Proc. Natl. Acad. Sci. USA* **111**, 13954–13959 (2014).
30. Duval, E. et al. Molecular mechanism of hypoxia-induced chondrogenesis and its application in in vivo cartilage tissue engineering. *Biomaterials* **33**, 6042–6051 (2012).
31. Graceffa, V. et al. Chasing chimeras—the elusive stable chondrogenic phenotype. *Biomaterials* **192**, 199–225 (2019).
32. Stegen, S. et al. HIF-1 alpha metabolically controls collagen synthesis and modification in chondrocytes. *Nature* **565**, 511–515 (2019).
33. Labuschagne, C. F., Cheung, E. C., Blagih, J., Domart, M. C. & Vousden, K. H. Cell clustering promotes a metabolic switch that supports metastatic colonization. *Cell Metab.* **30**, 720–734.e5 (2019).
34. Heiden, M. G. V., Cantley, L. C. & Thompson, C. B. Understanding the Warburg effect: the metabolic requirements of cell proliferation. *Science* **324**, 1029–1033 (2009).
35. Zhang, J. et al. Metabolism in pluripotent stem cells and early mammalian development. *Cell Metab.* **27**, 332–338 (2018).
36. Zheng, L. L., Zhang, Z. J., Sheng, P. Y. & Mobasheri, A. The role of metabolism in chondrocyte dysfunction and the progression of osteoarthritis. *Ageing Res. Rev.* **66**, 101249 (2021).
37. Duval, E. et al. Hypoxia-inducible factor 1 alpha inhibits the fibroblast-like markers type I and type III collagen during hypoxia-induced chondrocyte redifferentiation hypoxia not only induces type II collagen and aggrecan, but it also inhibits type I and type III collagen in the hypoxia-inducible factor 1 alpha-dependent redifferentiation of chondrocytes. *Arthritis Rheum.* **60**, 3038–3048 (2009).
38. Jeong, G. J. et al. Metabolites can regulate stem cell behavior through the STAT3/AKT pathway in a similar trend to that under hypoxic conditions. *Sci. Rep.* **9**, 6112 (2019).
39. Zhang, D. et al. Metabolic regulation of gene expression by histone lactylation. *Nature* **574**, 575–580 (2019).
40. Zhong, Y. et al. Dynamics of intrinsic glucose uptake kinetics in human mesenchymal stem cells during chondrogenesis. *Ann. Biomed. Eng.* **46**, 1896–1910 (2018).
41. Mahajan, A., Singh, A., Datta, D. & Katti, D. S. Bioinspired injectable hydrogels dynamically stiffen and contract to promote mechanosensing-mediated chondrogenic commitment of stem cells. *ACS Appl. Mater. Interfaces* **14**, 7531–7550 (2022).
42. Merkuri, F., Rothstein, M. & Simoes-Costa, M. Histone lactylation couples cellular metabolism with developmental gene regulatory networks. *Nat. Commun.* **15**, 90 (2024).
43. Arra, M. et al. LDHA-mediated ROS generation in chondrocytes is a potential therapeutic target for osteoarthritis. *Nat. Commun.* **11**, 3427 (2020).

44. Li, Y. Y., Lam, K. L., Chen, A. D., Zhang, W. & Chan, B. P. Collagen microencapsulation recapitulates mesenchymal condensation and potentiates chondrogenesis of human mesenchymal stem cells—a matrix-driven in vitro model of early skeletogenesis. *Biomaterials* **213**, 119210 (2019).
45. Liu, C. J. et al. Transcriptional activation of cartilage oligomeric matrix protein by Sox9, Sox5, and Sox6 transcription factors and CBP/p300 coactivators. *Front. Biosci.* **12**, 3899–3910 (2007).
46. Takács, R. et al. The temporal transcriptomic signature of cartilage formation. *Nucleic Acids Res.* **51**, 3590–3617 (2023).
47. Galeano-Garces, C. et al. Molecular validation of chondrogenic differentiation and hypoxia responsiveness of platelet-lysate expanded adipose tissue-derived human mesenchymal stromal cells. *Cartilage* **8**, 283–299 (2017).
48. Nosoudi, N. et al. Differentiation of adipose-derived stem cells to chondrocytes using electrospraying. *Sci. Rep.* **11**, 24301 (2021).
49. Kim, I. L., Mauck, R. L. & Burdick, J. A. Hydrogel design for cartilage tissue engineering: a case study with hyaluronic acid. *Biomaterials* **32**, 8771–8782 (2011).
50. Murphy, M. K., Huey, D. J., Hu, J. C. & Athanasiou, K. A. TGF-β1, GDF-5, and BMP-2 stimulation induces chondrogenesis in expanded human articular chondrocytes and marrow-derived stromal cells. *Stem Cells* **33**, 762–773 (2015).
51. Wei, K. C. et al. Robust biopolymeric supramolecular "Host-Guest Macromer" hydrogels reinforced by in situ formed multivalent nanoclusters for cartilage regeneration. *Macromolecules* **49**, 866–875 (2016).
52. Lin, W. F. & Klein, J. Recent progress in cartilage lubrication. *Adv. Mater.* **33**, e2005513 (2021).

Acknowledgements

This work was supported by the National Key R&D Program of China (2022YFB3804403, L.B.). This work was supported by the National Natural Science Foundation of China (52433010, L.B.). This work was supported by the Collaborative Research Fund from the Research Grants Council of Hong Kong (C5044-21G, L.B.). This work was financially supported by the GJYC Program of Guangzhou (2024D03J0004, L.B.; 2024D01J0084, K.Z.). This work was also financially supported by the Guangzhou Basic and Applied Basic Research Foundation (2023A04J1472, K.Z.) and the Fundamental Research Funds for the Central Universities (2024ZYGXZR086, K.Z.).

Author contributions

L.B., K.Z., B.Y., and Z.L. designed the study, conducted the analysis, provided discussion, and prepared the manuscript; B.Y., X.X., P.Z., X.Y., and Z.N.Y. synthesized hydrogels and investigated the physical and chemical properties of materials; J.W., W.L., and T.N. designed and investigated the microrheological properties of hydrogels; B.Y. and Y.L. conducted the SPR experiment; S.L., Z.M.Y., Z.Z. and G.L. designed and conducted the animal experiments, and analyzed the results of animal experiments.

Competing interests

The authors declare no competing interests.

Additional information

Supplementary information The online version contains supplementary material available at https://doi.org/10.1038/s41467-025-57779-6.

Correspondence and requests for materials should be addressed to To Ngai, Kunyu Zhang or Liming Bian.

Peer review information *Nature Communications* thanks the anonymous reviewers for their contribution to the peer review of this work. A peer review file is available.

Reprints and permissions information is available at http://www.nature.com/reprints

Publisher's note Springer Nature remains neutral with regard to jurisdictional claims in published maps and institutional affiliations.

[1]Department of Biomedical Engineering, The Chinese University of Hong Kong, Hong Kong SAR, PR China. [2]Department of Orthopaedics and Traumatology, Faculty of Medicine, The Chinese University of Hong Kong, Hong Kong SAR, PR China. [3]School of Biomedical Sciences and Engineering, Guangzhou International Campus, South China University of Technology, Guangzhou, PR China. [4]National Engineering Research Center for Tissue Restoration and Reconstruction, South China University of Technology, Guangzhou, PR China. [5]Guangdong Provincial Key Laboratory of Biomedical Engineering, South China University of Technology, Guangzhou, PR China. [6]Department of Chemistry, The Chinese University of Hong Kong, Hong Kong SAR, PR China. [7]Engineering Research Center for Biomedical Materials, Anhui Key Laboratory of Modern Biomanufacturing, School of Life Sciences, Anhui University, Hefei, Anhui Province, PR China. [8]These authors contributed equally: Boguang Yang, Zhuo Li, Zhengmeng Yang. ✉e-mail: tongai@cuhk.edu.hk; kyuzhang@scut.edu.cn; bianlm@scut.edu.cn